Supporting Information

Freestanding MXene-hydrogel *via* critical density controlled self-assembly: high performance energy storage with ultrahigh capacitive vs diffusion limited contribution

Pronoy Dutta, Amalika Patra, Sujit Kumar Deb, Anirban Sikdar, Abhisek Majumdar , Golam Masud Karim, Uday Narayan Maiti *

Department of Physics, Indian Institute of Technology Guwahati, Guwahati-781039, Assam, India

Corresponding address:

udaymaiti@iitg.ac.in (UNM)

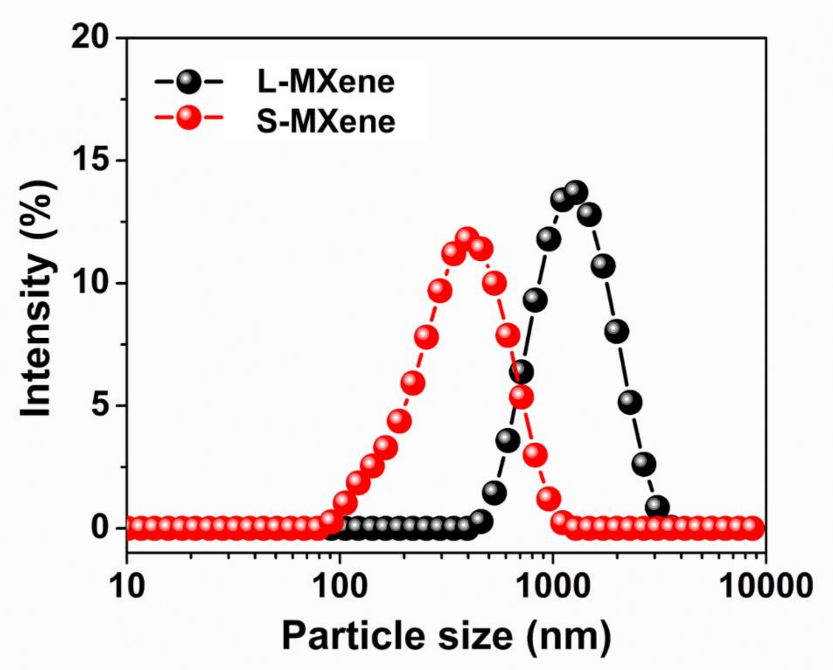

Fig. S1: DLS measurement of large and small MXene dispersion indicating the sheet size distribution

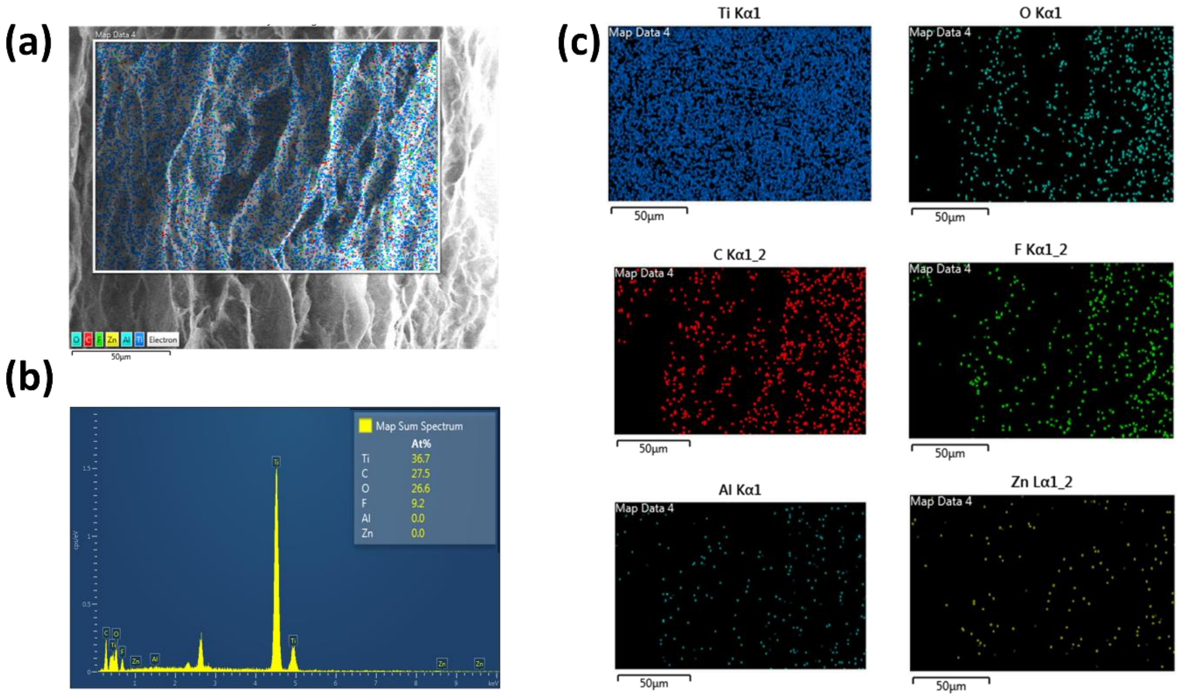

Fig. S2: Cross sectional FESEM EDS spectra of freeze-dried MXene hydrogel: (a) Mapping of different elements over the hydrogel cross section; (b) corresponding at% and (c) mapping of individual elements over the structure.

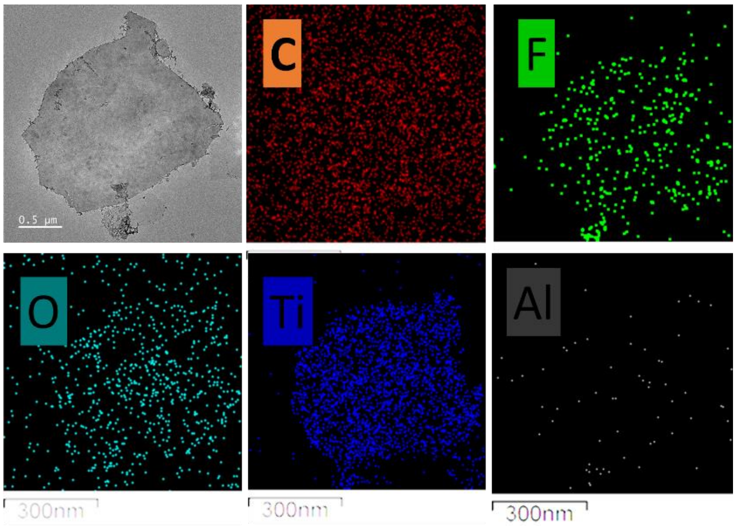

Fig. S3: FETEM image of MXene flake with corresponding EDS spectra confirming subsequent etching of Al and functionalization in the MILD etching process.

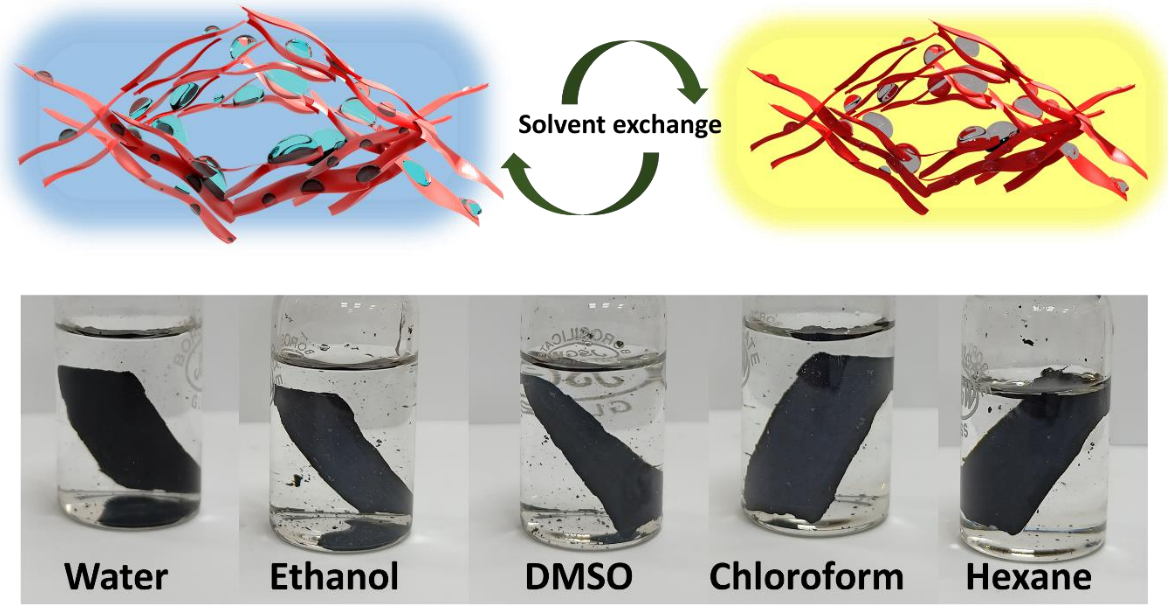

Fig. S4: Facile solvent exchange in MXene hydrogels for the development of possible solvated MXene framework (SMF).

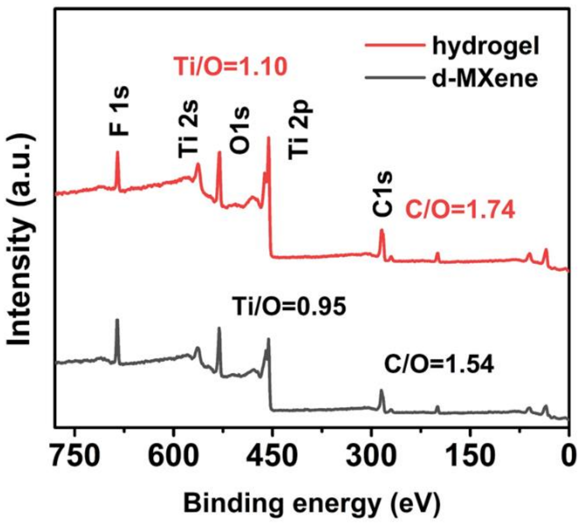

Fig. S5: XPS survey scan for d-MXene and MXene hydrogel.

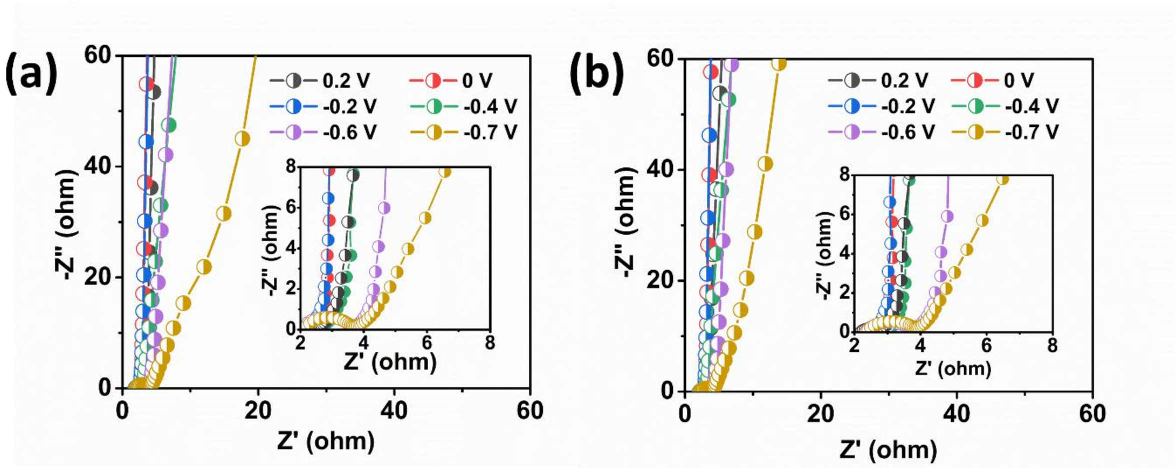

Fig. S6: EIS spectra of hydrogels at different applied potentials for (a) LMH_3.1, (b) SMH_3.4 electrodes.

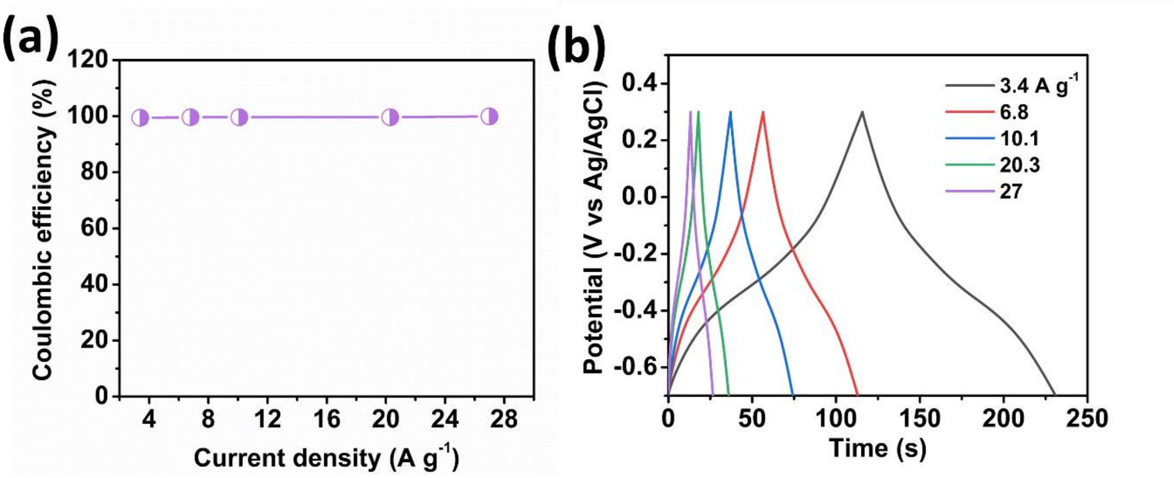

Fig. S7: (a) Coulombic efficiency and (b) GCD curves at different current densities for LMH_3.1 electrode.

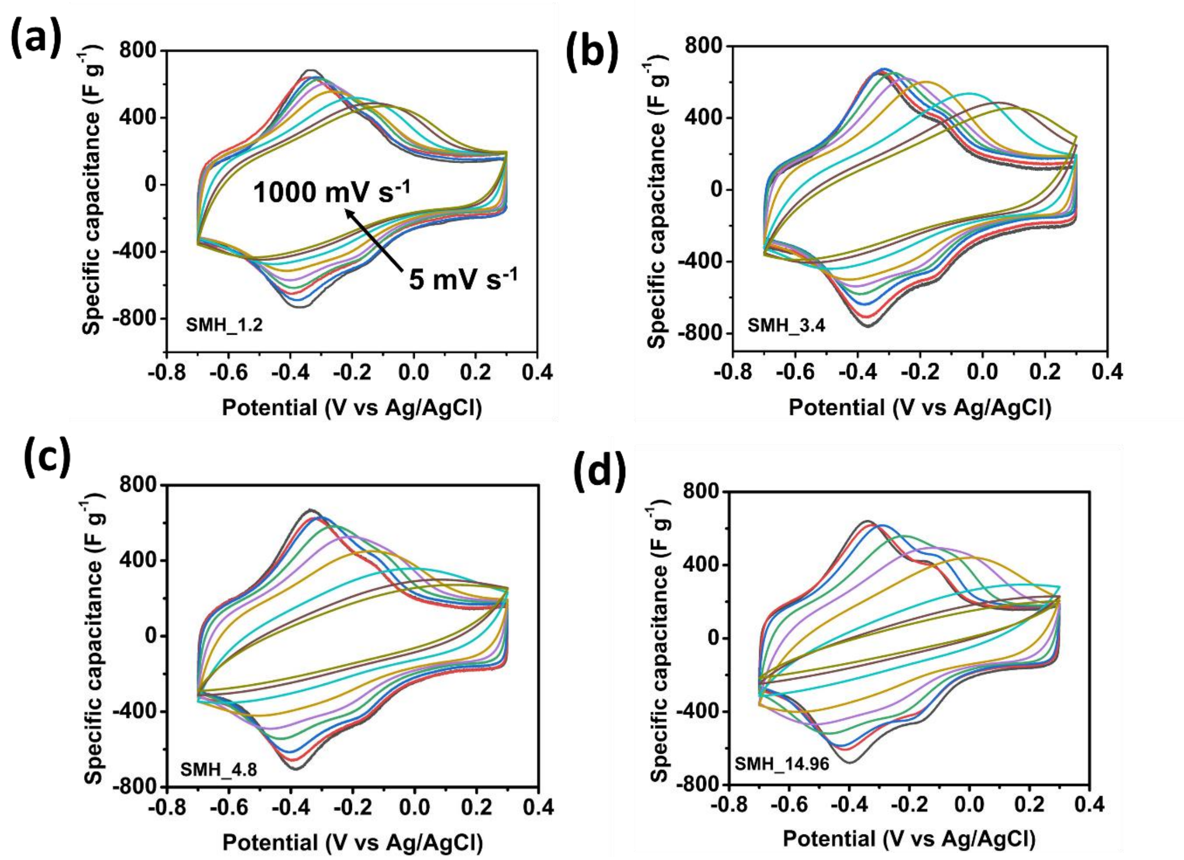

Fig. S8: CV curves of SMH electrodes of different mass loading at scan rates from 5 mV s^{-1} to 1000 mV s^{-1}

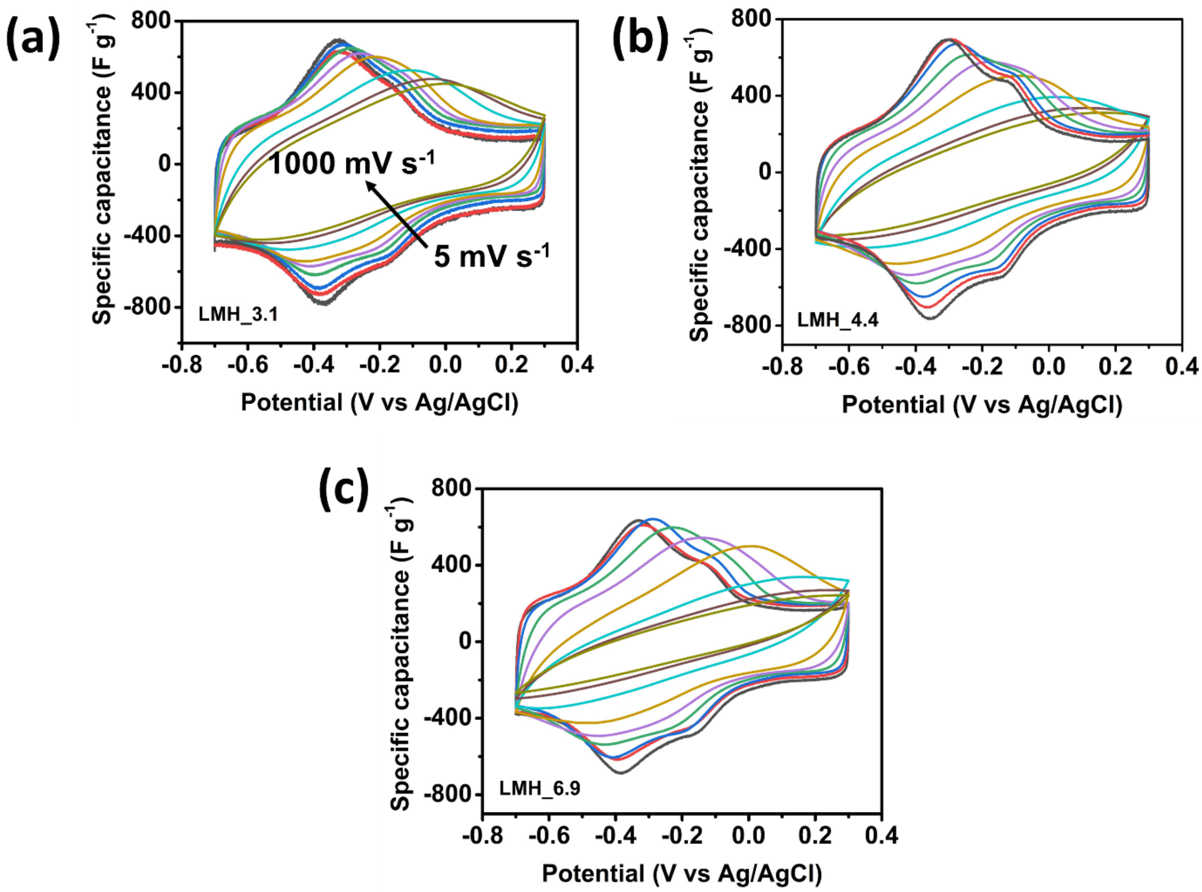

Fig. S9: CV curves of LMH electrodes of different mass loading at scan rates from 5 mV s^{-1} to 1000 mV s^{-1}

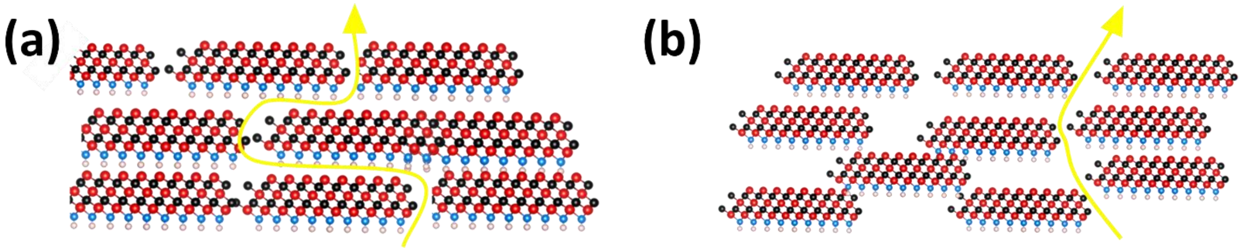

Fig. S10: Illustration for difference in ion transportation in large and small sheet hydrogels. (a) hydrogels with large sheet size increases the diffusion path whereas regular ion transport channels ease the transportability in (b) small sheet hydrogels

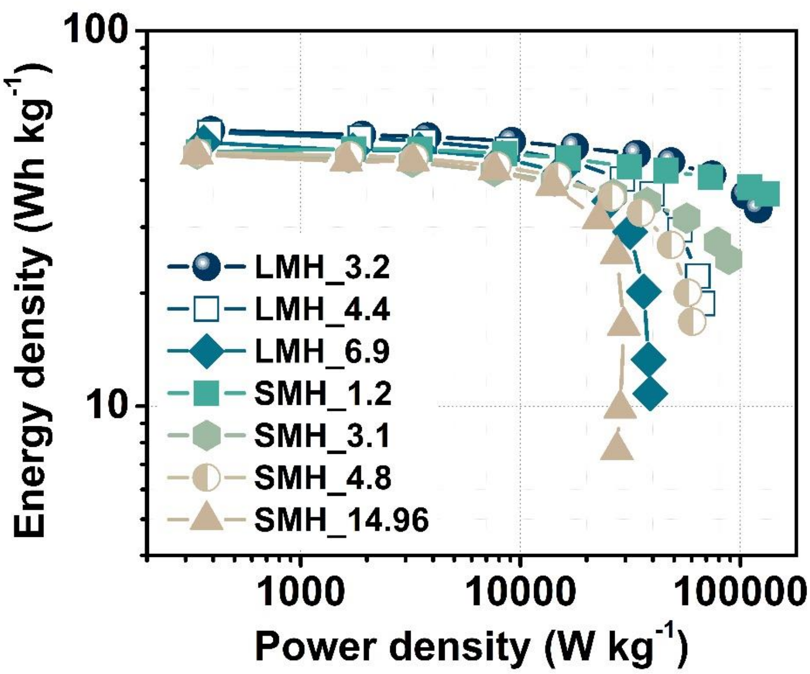

Fig. S11: Regone plot showing gravimetric energy and power densities of freestanding hydrogel electrodes.

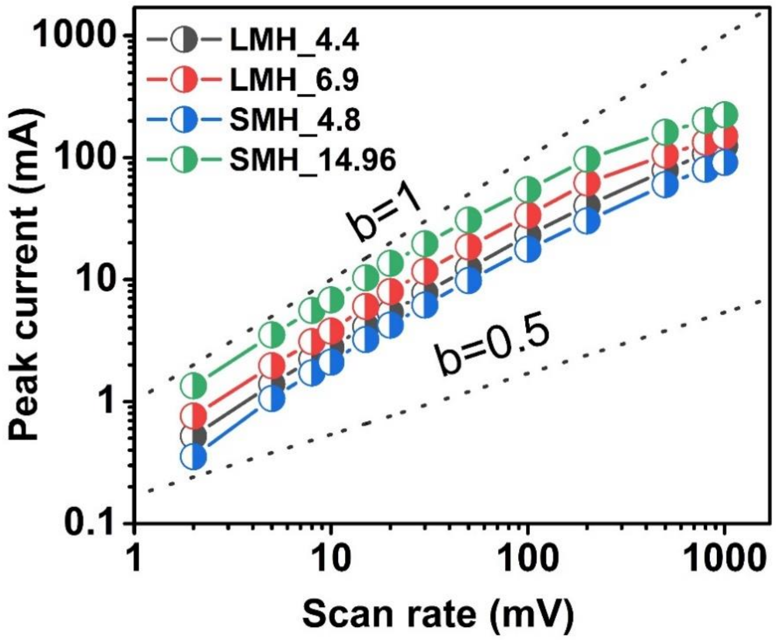

Fig. S12: *b* values of MXene hydrogels determined from power law.

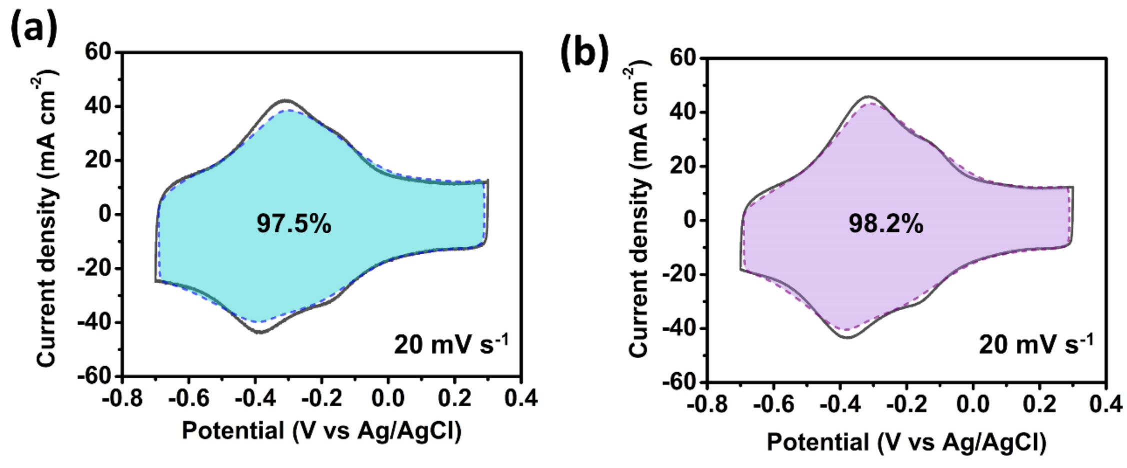

Fig. S13: Analysis for capacitive contribution in charge storage for MXene hydrogels at 20 mV s^{-1}: (a) For LMH_3.1 and (b) SMH_3.4 hydrogel electrode.

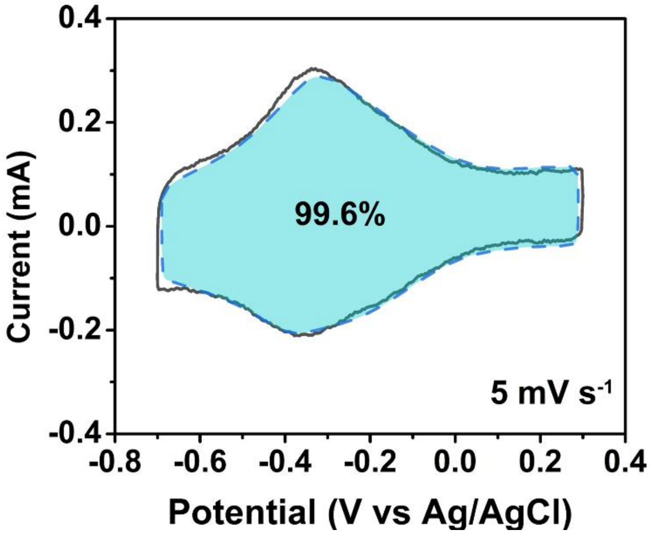

Fig. S14: Analysis of capacitive contribution in compressed SCMH-3.6 electrode at 5 mV s^{-1}.

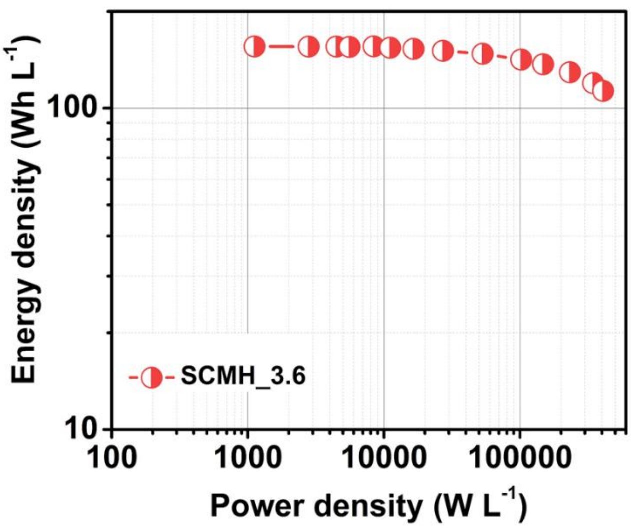

Fig. S15: Regone plot for volumetric energy and power densities for the electrolyte assisted compressed SCMH_3.6 electrode.

Table S1: List of MXene hydrogel samples and their energy storage matrices calculated from CV curves at 2 mV s^{-1}.

Sample name	Mass loading (mg cm^{-2})	Gravimetric capacitance (F g^{-1})	Areal capacitance (mF cm^{-2})
LMH_3.1	3.1	391.01	1212.1
LMH_4.4	4.4	386.33	1699.85
LMH_6.9	6.9	363.05	2505.07
SMH_1.2	1.2	342.57	411.09
SMH_3.4	3.4	344.76	1168.73
SMH_4.8	4.8	340.65	1635.12
SMH_14.96	14.96	337.08	5042.81

Table S2: Electrochemical performance comparison of freestanding MXene hydrogels with previously reported MXene based electrodes.

Sample type	Gravimetric capacitance (F/g)	Mass loading	Rate performance	Electrolyte	Reference
$Ti_3C_2T_x$ clay	245 Fg^{-1} at 2 mV s^{-1}	-	80% @ 100 mV s^{-1}	1 M H_2SO_4	1
$Ti_3C_2T_x$ film	195 Fg^{-1} at 2 mV s^{-1}	0.75mg cm^{-2}	61% @ 1 V s^{-1}	LiTFSI–PC	2
d-Ti_3C_2 film	325 Fg^{-1} at 2 mV s^{-1}	1.3 mg cm^{-2}	42.3% @ 100 mV s^{-1}	1M H_2SO_4	3
Rolled MXene aerogel	315 Fg^{-1} at 10 mV s^{-1}	0.6 mg cm^{-2}	39% at 200 mV s^{-1}	3M H_2SO_4	4
Alkali treated $Ti_3C_2T_x$	314 Fg^{-1} at 2 mV s^{-1}	8.5 mg cm^{-2}	-	1M H_2SO_4	5
Cation intercalated $Ti_3C_2T_x$	130 Fg^{-1} at 2 mV s^{-1}	-	61.5% at 100	1M KOH	6
$Ti_3C_2T_x$-rGO film	391 Fg^{-1} at 2 mV s^{-1}	-	49 % at 1 V s^{-1}	3M H_2SO_4	7
rGO/$Ti_3C_2T_x$ film	335.4 Fg^{-1} at 2 mV s^{-1}	-	61% @ 1 V s^{-1}	3M H_2SO_4	8
$Ti_3C_2T_x$-SWCNT	134 Fg^{-1} at 2 mV s^{-1}	0.73	71.8 at 200	1M $MgSO_4$	9
***d*-Mo_2CT_x film**	196 Fg^{-1} @ 2 mV s^{-1}	0.6mg cm^{-2}	61.2 at 100	1M H_2SO_4	10
$Ti_3C_2T_x$-PVA	167 Fg^{-1} at 2 mV s^{-1}	-	56.8 at 100	1M KOH	11
LMH_3.1	391 Fg^{-1} at 2 mV s^{-1}	3.1	60% at 1 V s^{-1}	3M H_2SO_4	This work
SMH_1.2	342.6 Fg^{-1} at 2 mV s^{-1}	1.2	76% at 1 V s^{-1}	3M H_2SO_4	This work
SMH_14.96	337.08 Fg^{-1} at 2 mV s^{-1}	14.96	82% at 100 mV s^{-1}	3M H_2SO_4	This work

Tables S3: ESR values of MXene hydrogels:

Sample name	ESR (Ω)
LMH_3.1	1.64
LMH_6.9	2.58
SMH_1.2	1.39
SMH_3.4	1.38
SMH_14.96	1.45

Table S4: Comparison of surface capacitive contribution in MXene based electrodes:

Sample	Surface capacitive contribution	Reference
$Ti_3C_2T_x$ aerogel	60.1% at 2 mV s^{-1}	[12]
Pristine $Ti_3C_2T_x$	87.2% at 10 mV s^{-1}	[13]
N doped $Ti_3C_2T_x$ film	65.5% at 10 mV s^{-1}	[13]
MXene/PANI film electrodes	82% at 2 mV s^{-1}	[14]
Large sheet $Ti_3C_2T_x$ films	66.5% at 5 mV s^{-1}	[15]
Small sheet etched $Ti_3C_2T_x$ films	90.5% at 5 mV s^{-1}	[15]
LMH_3.3	94.3% at 5 mV s^{-1}	This work
SMH_3.1	96% at 5 mV s^{-1}	This work

References

1 M. Ghidiu, M. R. Lukatskaya, M.-Q. Zhao, Y. Gogotsi and M. W. Barsoum, *Nature*, , DOI:10.1038/nature13970.

2 X. Wang, T. S. Mathis, K. Li, Z. Lin, L. Vlcek, T. Torita, N. C. Osti, C. Hatter, P. Urbankowski, A. Sarycheva, M. Tyagi, E. Mamontov, P. Simon and Y. Gogotsi, *Nat. Energy*, , DOI:10.1038/s41560-019-0339-9.

3 Y. Dall'Agnese, M. R. Lukatskaya, K. M. Cook, P. L. Taberna, Y. Gogotsi and P. Simon, *Electrochem. commun.*, 2014, **48**, 118–122.

4 V. Bayram, M. Ghidiu, J. J. Byun, S. D. Rawson, P. Yang, S. A. Mcdonald, M. Lindley, S. Fairclough, S. J. Haigh, P. J. Withers, M. W. Barsoum, I. A. Kinloch and S. Barg, *ACS Appl. Energy Mater.*, 2019, **3**, 411–422.

5 T. Li, L. Ulu Yao, I. Liu, J. Gu, R. Luo, J. Inghan Li, X. Yan, W. Wang, P. Liu, B. Chen, W. Zhang, W. Abbas, R. Naz and D. Zhang, , DOI:10.1002/ange.201800887.

6 M. R. Lukatskaya, O. Mashtalir, C. E. Ren, Y. Dall'Agnese, P. Rozier, P. L. Taberna, M. Naguib, P. Simon, M. W. Barsoum and Y. Gogotsi, *Science (80-.).*, 2013, **341**, 1502–1505.

7 G. Wu, O. Li, Z. Wang, M. Li, B. Wang and A. Dong, , DOI:10.1002/anie.202009086.

8 J. Yan, C. E. Ren, K. Maleski, C. B. Hatter, B. Anasori, P. Urbankowski, A. Sarycheva and Y. Gogotsi, *Adv. Funct. Mater.*, 2017, **27**, 1701264.

9 M.-Q. Zhao, C. E. Ren, Z. Ling, M. R. Lukatskaya, C. Zhang, K. L. Van Aken, M. W. Barsoum and Y. Gogotsi, *Adv. Mater.*, 2015, **27**, 339–345.

10 J. Halim, S. Kota, M. R. Lukatskaya, M. Naguib, M.-Q. Zhao, E. Ju Moon, J. Pitock, J. Nanda, S. J. May, Y. Gogotsi, M. W. Barsoum, J. Halim, S. Kota, M. R. Lukatskaya, M. Q. Zhao, E. J. Moon, J. Pitock, S. J. May, Y. Gogotsi, M. W. Barsoum and Y. A. Gogotsi J, , DOI:10.1002/adfm.201505328.

11 Z. Ling, C. E. Ren, M.-Q. Zhao, J. Yang, J. M. Giammarco, J. Qiu, M. W. Barsoum and Y. Gogotsi, *Proc. Natl. Acad. Sci.*, 2014, **111**, 16676–16681.

12 V. Bayram, M. Ghidiu, J. J. Byun, S. D. Rawson, P. Yang, S. A. Mcdonald, M. Lindley, S. Fairclough, S. J. Haigh, P. J. Withers, M. W. Barsoum, I. A. Kinloch, S.

Barg and U. K. 9pl, 2021, **10**, 16.

13 Y. Tian, W. Que, Y. Luo, C. Yang, X. Yin and L. B. Kong, , DOI:10.1039/c9ta00076c.

14 A. Vahidmohammadi, J. Moncada, H. Chen, E. Kayali, J. Orangi, C. A. Carrero and M. Beidaghi, *J. Mater. Chem. A*, 2018, **6**, 22123–22133.

15 J. Tang, T. Mathis, X. Zhong, X. Xiao, H. Wang, M. Anayee, F. Pan, B. Xu and Y. Gogotsi, *Adv. Energy Mater.*, 2020, 2003025.